Fault Current Control for DC Microgrid Protection Using an Adaptive Droop

Sijo Augustine*, Sukumar M. Brahma†, Matthew J. Reno‡
*Klipsch School of Electrical Computer Engineering, New Mexico State University, USA
†Holcombe Department of Electrical Computer Engineering, Clemson University, USA
‡Electric Power Systems Research, Sandia National Laboratories, USA

***Abstract*—Successful system protection is critical to the performance of the DC microgrid system. This paper proposes an adaptive droop based fault current control for a standalone low voltage (LV) solar-photovoltaic (PV) based DC microgrid protection. In the proposed method, a DC microgrid fault is detected by the current and voltage thresholds. Generally, the droop method is used to control the power sharing between the converters by controlling the reference voltage. In this paper, this scheme is extended to control the fault current by calculating an adaptive virtual resistance R_{droop}, and to control the converter output reference voltage. This effectively controls the converter pulse width, and reduces the flow of source current from a particular converter which helps to increase the fault clearing time. Additionally, a trip signal is sent to the corresponding DC circuit breaker (DCCB), to isolate the faulted converter, feeder or a DC bus. The design procedure is detailed, and the effectiveness of proposed method is verified by simulation analysis.**

***Index Terms*—DC Microgrid, droop control, fault current, islanded, low voltage, protection, solar-PV, voltage control.**

I. Introduction

Currently, the distribution systems are increasingly utilizing DC components and associated power electronics interfaces. Consequently, DC microgrids are emerging as an attractive solution allowing customers to maintain electrical service independent of the main grid. Microgrids also enable customers to generate, control, and store energy. These aspects additionally present customers some potential economic benefits for local power generation [1], [2]. The major concerns related to the design and control of DC microgrids are the selection of converter topologies, maximum power point tracking (MPPT), voltage control, power sharing, energy management and protection [3]. Considering system components and configurations, faults in a solar-PV DC microgrid system are classified as either short circuit (line-line and line-ground) or PV arc faults [4].

Generally, a DC microgrid covers a small geographical area and the distribution line length is short compared to AC distribution systems. Therefore, DC microgrids can be treated as resistive networks [5]. Unlike conventional power system generators, microgrids utilize power electronic converters to integrate energy sources like solar-PV, wind, fuel cells, microturbines, energy storage devices, and loads. In standalone mode, small-scale distribution generators and inverted DC sources offer little to no rotational inertia, and this affects the system stability during disturbances or faults. DC microgrid disturbances are mainly due to fluctuations in load, input power variations, changes in load sharing proportions, oscillations in MPPT [6], temporary faults, communication failures or delays, disturbances in the AC grid. These technical and operational issues have potential to degrade the system performance. Therefore, DC microgrid protection is a critical component for safety, reliability, and asset protection. The objectives for DC microgrid protection are reliability, speed, selectivity, simplicity and cost [7].

One of the major challenges associated with DC microgrid protection is the fault clearing time. Fault clearing time depends on (i) system configuration and converter topologies (ii) fault location (iii) signal processing and communication delay and (iv) speed of DCCB's [8]. In a DC microgrid, the capacitive filters connected to the output side of the converters will rapidly discharge into a fault, resulting in large current surges within a very short duration. This may lead to an unstable operation of the converters, since the converters are designed to operate in some particular voltage range. Therefore, this paper focuses on the control of fault current in an islanded DC microgrid to increase the fault clearing time.

As discussed in [4], [8]–[16], the simplest and most cost effective method for microgrid protection involves using the voltage and current thresholds. For example, when a fault occurs, there is a drop in the bus voltage and a rise in the converter current. These changes are used to generate a trip signal by comparing the magnitudes of these signals to some predefined thresholds. This method relies solely on current and voltage magnitudes, allowing for fast fault detection. Another scheme in this category is the active impedance method detailed in [13], [14]. In this method, if there is any abnormality in the system the circuit injects a short-duration spread frequency current spikes to estimate the line impedance. The main drawback of this scheme is the accuracy of the estimated fault location and it may vary with the sensing parameters and mathematical formulations derived. Also, the cost of the system increases with the number of probing arrangements in multiple locations and high bandwidth sensing units. A non-iterative fault detection scheme is proposed for LVDC microgrid systems in [15]. The algorithm involves using an external probe unit to analyze the fault without the need to de-energize the system. The power probe unit consists of a power source, capacitor, inductor and CB's. In this method, the DC microgrid is divided into zones. If a fault occurs, intelligent electronic devices (IEDs) are used to detect and

isolate the fault location based on the predefined thresholds. A combination of voltage and current derivative-based fault detection scheme is described in [16]. This method uses the current direction, rate of change of currents and rate of change of voltages information to detect the fault. This helps to classify the faults as internal or external. For example, during a cable fault, a positive current derivative shows the fault is within the protection zone and a negative current derivative indicates an external fault. Difficulty to classify the transients and faults is the main drawback of this algorithm.

II. System Configuration

A standalone 4-bus DC microgrid system is shown in Fig. 1. Each bus consists of two solar-PV boost converters, one bidirectional converter for battery and one converter for DC loads. A detailed connection of converters at bus#1 is shown in Fig. 2(a). Where V_{DC1}, V_{DC2}, V_{B1}, I_{pv1}, I_{pv2}, I_{B1}, R_{pv1}, R_{pv2} and R_{B1} represents the output voltages, currents and cable resistances of converter-1, converter-2 and bidirectional converter-1. Also, the individual converter power at any instant is represented as P_{pv1}, P_{pv2} and P_{B1}. F_1 and F_2 are the line-line fault locations considered in the proposed algorithm.

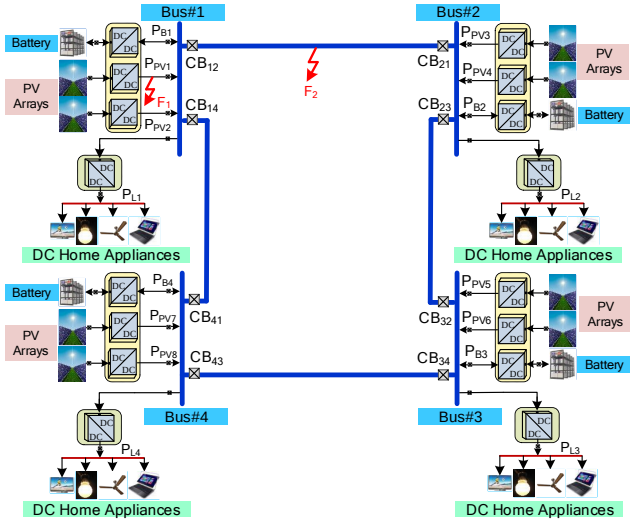

Fig. 1. Schematic representation of a 4-bus DC microgrid system.

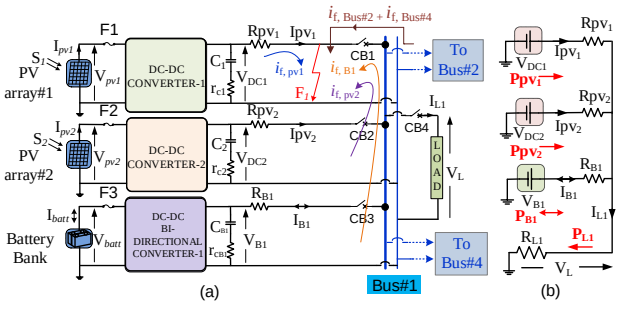

Fig. 2. (a) Detailed schematic representation of bus#1 with a line-line cable fault, and (b) Steady state equivalent circuit for the DC output side.

The output side of the converter can be represented as a voltage source in series with its cable resistances and the equivalent circuit is shown in Fig. 2(b).

If a line-line cable fault (F_1) occurs at converter-1 as shown in Fig. 2(a), the total fault current can be calculated as,

$$i_f = i_{f,pv1} + i_{f,pv2} + i_{f,B1} + i_{f,Bus\#2} + i_{f,Bus\#4}, \quad (1)$$

where,

$$|i_{f,pv1}| > |i_{f,pv2}|, |i_{f,B1}|, |i_{f,Bus\#2}|, |i_{f,Bus\#4}|.$$

Converter-1's contribution to the fault current can be divided into two components: (i) the fault current component from the DC power source and (ii) the current from the DC bus capacitor. The fault current component from the solar-PV source is,

$$i_{f,pv1_{PV}}(t) = \frac{V_{pv}}{R_{eq}}\left[1 - e^{\left[\frac{-t}{\tau_1}\right]}\right], \quad (2)$$

where, τ_1 is the time constant of the converter-1 source fault current and depends on the line reactance. In the similar way the capacitor component can be expressed as,

$$i_{f,pv1_{Capa}}(t) = \frac{V_C}{R_{ESR}}\left[e^{\left[\frac{-t}{\tau_2}\right]}\right], \quad (3)$$

where, τ_2 is the time constant of the converter-1 capacitor fault current component and depends on the equivalent series resistance (ESR) and capacitance of the DC bus capacitor. It should be noted that due to the small scale of the time constant, the component of the fault current due to the DC capacitor can rapidly ramp to relatively large magnitudes. Converter-1 fault current contribution during F_1 is shown in Fig. 3. It is observed that within 20 μs, the converter-1 fault current reaches a maximum of approximately 50 A, and the capacitor current contribution is approximately 40 A. From the above

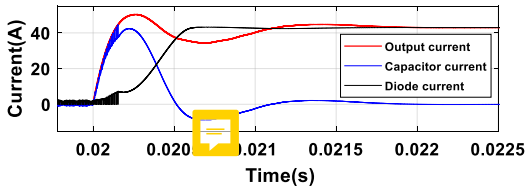

Fig. 3. Fault current contribution of converter-1 during F_1.

discussion, it can be concluded that the source component and the capacitor component should be controlled for the safe operation of the converter during the fault. The proposed fault current control method is introduced in the next section.

III. Proposed Fault Current Control Algorithm

This section explains the operation of the converter during fault by using the droop method. For the desired power sharing, the converters' output voltages and input currents can be controlled by adjusting the reference voltage of each converter. This can be extended for controlling the converter fault current. In order to achieve this, during fault conditions the reference voltage of each converter is controlled by using the virtual impedance R_{droop} [17] and is shown in Fig. 4. This can be achieved by taking the output current feedback from the converter and multiplied with the calculated R_{droop}. This

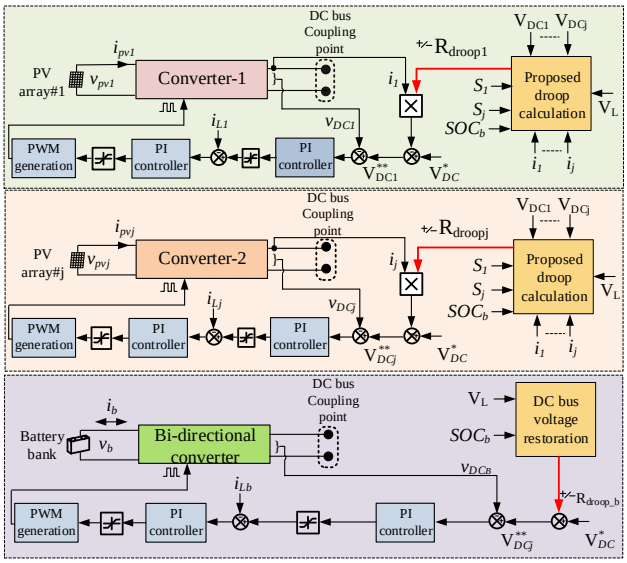

Fig. 4. Control diagram of bus#1 converters with the proposed algorithm.

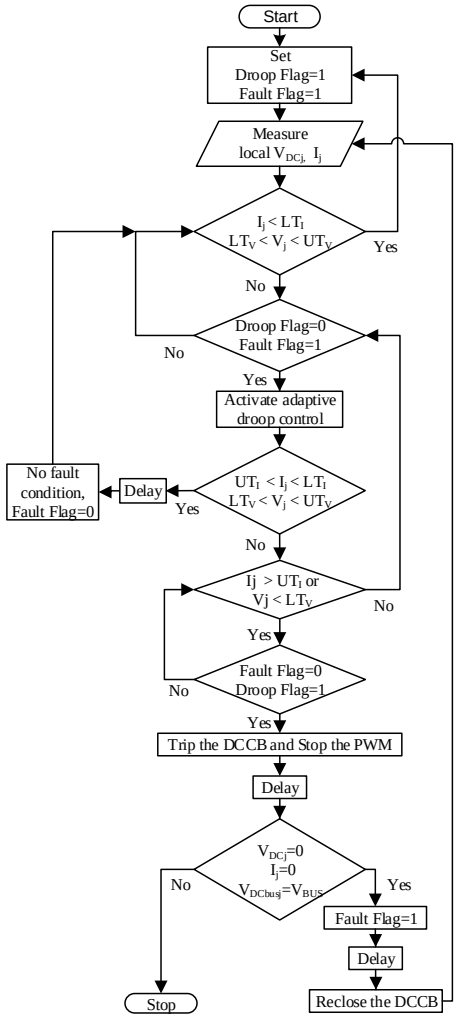

Fig. 5. Flowchart for converter-j $(j = 1, 2..n)$ fault protection algorithm.

resultant signal is subtracted from the reference voltage (V^*_{DC}) of the converter and the new reference signal is now (V^{**}_{DCj}) and is given as,

$$V^{**}_{DCj} = V^*_{DC} - i_j \times (\pm R_{droop_j}). \quad (4)$$

In the proposed adaptive droop based algorithm, the fault detection is based on the voltage and current thresholds. Using the proposed adaptive droop protection method, the output converter voltage is controlled during the fault. Therefore, the complete shutdown of the DC microgrid may not be required during the fault. This can be explained with Fig. 1. In the considered system each bus consists of six CB's and all converters and loads can be isolated based on the fault location. The proposed protection schemes consist of main protection and backup protection schemes. The algorithm is discussed as follows, and the flowcharts are given in Fig. 5 and Fig. 6.

1) The thresholds are calculated based on the converter topology, rating, DC bus voltage limits and load parameters. In the proposed method, the current thresholds are based on converter current rating, topology and voltage thresholds defined by the allowable limits of DC grid voltage. These current thresholds are selected by considering the converter input current or device (MOSFET or IGBT) current or the output current. If the current or voltage magnitude crosses the threshold, the controller activates the proposed algorithm and and a trip signal is sent to the DCCB if necessary.
2) The implementation of the proposed algorithm is based on two current thresholds and two voltage thresholds, an upper threshold (UT_I & UT_V) and a lower threshold (LT_I & LT_V) as shown in Fig. 7. For example, the upper current threshold can be selected as 150% of the full load current and the lower threshold as 120% of the full load value. Similarly, the voltage thresholds are based on the allowable DC bus voltage deviation. If the DC bus voltage is 48 V, then the thresholds can be selected as $48 \pm 2.5\% V$ (lower threshold) and $48 \pm 20\% V$(upper threshold). It should be noted that a small change in the converter output voltage will affect the current sharing proportion among the converters.
3) The proposed method is activated only if the current or voltage magnitude crosses lower threshold as shown in Fig. 7. If the current magnitude crosses the lower threshold, the algorithm identifies that there is chance of disturbance or fault.
4) The adaptive droop algorithm adjusts the converter output voltage and reduces the total converter output current. If the current again exceeds the threshold UT_I, then the algorithm generates a trip signal to the particular DCCB.

IV. Simulation Studies

The 4-bus DC microgrid system as shown in the Fig. 1 was simulated, using MATLAB/Simulink. The nominal parameters

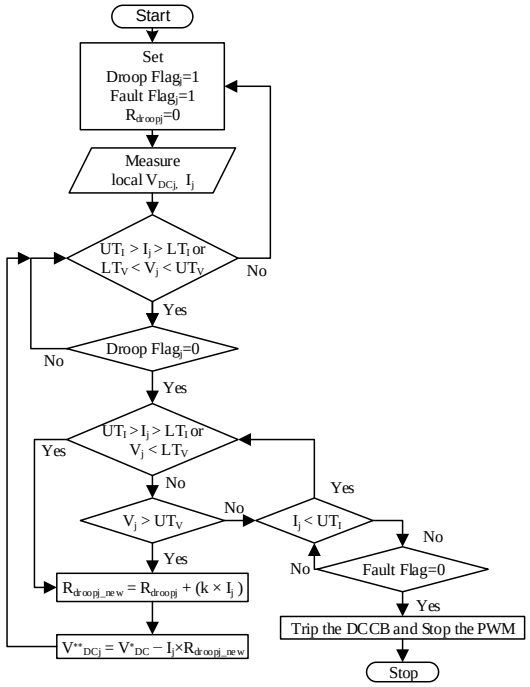

Fig. 6. Flowchart for converter-j $(j = 1, 2..n)$ adaptive droop algorithm.

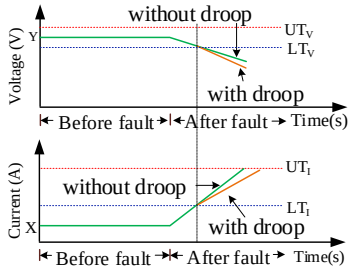

Fig. 7. Voltage and current profile of converter-j $(j = 1, 2..n)$ with and without adaptive droop algorithm.

of the system are given in the Table I.

TABLE I
NOMINAL PARAMETERS OF SYSTEM

Parameters	Symbol	Value
DC bus voltage	V_{DC}	48 V
Boost converter power	P_{boost}	240 W
Battery converter power	P_{batt}	240 W
Cable resistance	R_{cable}	0.1 Ω
Cable inductance	L_{cable}	0.1 mH
Filter inductor	L	100 μH
ESR of filter inductor	r_L	0.03 Ω
Filter capacitor	C	440 μF
ESR of filter capacitor	r_C	0.05 Ω
Nominal switching frequency	f_{sw}	10 kHz

A. Normal operation of the DC microgrid

The normal operation of the DC microgrid is simulated and the voltages and currents are shown in Fig. 8. The converter output voltages and load voltage are shown in the Fig. 8(a).

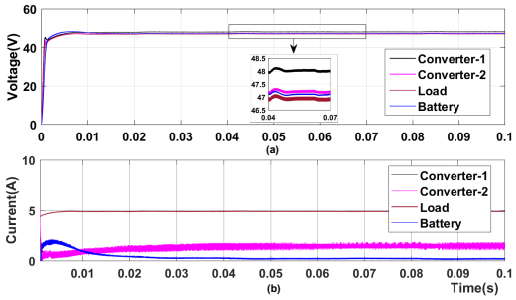

Fig. 8. Voltage and current of bus#1 converters during normal operation.

It can be observed in Fig. 8(b) that the PV converters each contribute 2.2 A to the total 5 A load current. The remaining portion of the load current is contributed by the battery converter.

B. Cable fault (F_1) with adaptive droop algorithm

At 0.02 s, a line-line fault is created in the converter-1 to bus#1 cable. The corresponding simulation results are shown in Fig. 9. The proposed adaptive droop control is implemented, and the voltage and current thresholds are defined in Table II. Fig. 9(a) shows the converter-1 output voltage and the reference voltage. The converter-1 output current is shown in Fig. 9(b). The droop flag is activated when output current reaches 6 A, and the droop values are shown in the Fig. 9(d). The change in the converter-1 reference voltage as shown in the the Fig. 9(a) controls the fault current contribution from converter-1.

TABLE II
VOLTAGE AND CURRENT THRESHOLDS

Parameter	Magnitude	
Voltage	UT_V = 46 V	LT_V = 35 V
Current	UT_I = 10 A	LT_I = 6 A

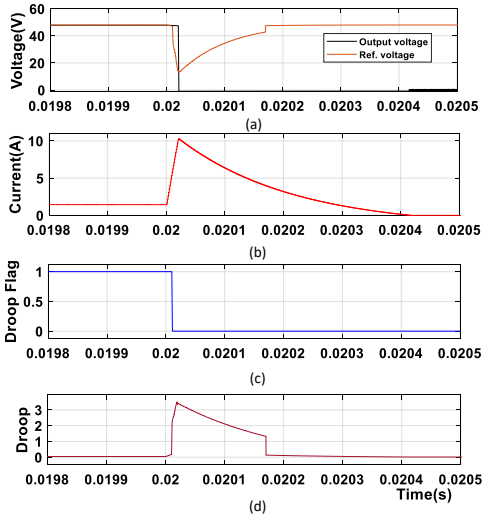

Fig. 9. Converter-1 results for fault F_1 at 0.02 s (a) Output voltage (b) Output current (c) Droop flag (d) Calculated adaptive droop.

The simulation results of converter-2 are shown in the Fig. 10. It can be observed from Fig. 10(a) that the converter maintains the output voltage at 48 V. In Fig. 10(b), at 0.02 s it can be seen that the current out of converter-2 peaks at approximately 3 A, and the droop flag remains unchanged as shown in the Fig. 10(c). The deviation in the calculated adaptive droop value seen in Fig. 10(d) is due to this rise in current. The droop values are activated when the converter-1 current exceeds $LT_I = 6\,A$ and deactivates when it drops below the same magnitude.

The corresponding bus#1 voltage is shown in Fig. 11. During the fault, it can be observed that the maximum fluctuation in the voltage is approximately $12\,\%$ for a duration of $2\,\mu$s.

Fig. 12 shows the converter-1 behavior during the fault (F_1) at 0.02 s without adaptive droop control. The adaptive droop values are zero during the fault and is shown in Fig. 12(a). It can be observed from Fig. 12(b, c, d) that the magnitude of source or inductor current, MOSFET current and diode current increase after 0.02 s. When the total converter-1 current reaches 10 A (UT_I), the algorithm generates a trip signal and isolates the faulted zone from the DC microgrid. Fig. 13 shows the converter-1 behavior during the fault with the proposed control. The adaptive droop values are shown in Fig. 13(a). It can be additionally observed from Fig. 13(b, c, d) that after the droop activation, the magnitude of inductor current, MOSFET current and diode current decrease.

As discussed in the Section II, 10 A is selected as the source current threshold instead of converter-1 output current threshold. The results without utilizing the proposed control

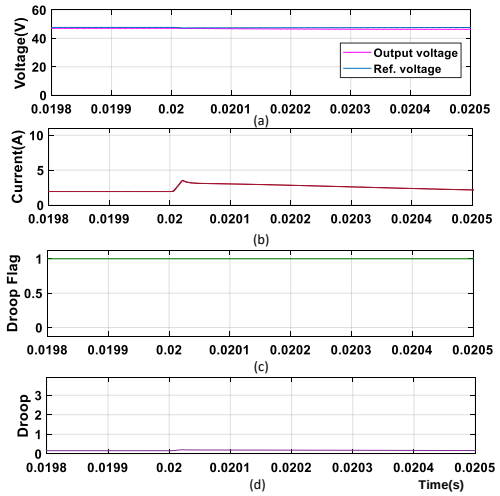

Fig. 10. Converter-1 results for fault F_1 at 0.02 s (a) Output voltage (b) Output current (c) Droop flag (d) Calculated adaptive droop.

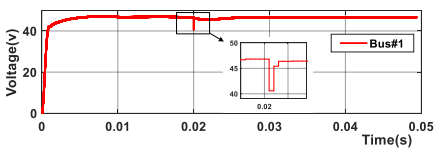

Fig. 11. Variation of bus#1 voltage during F_1 at 0.02s.

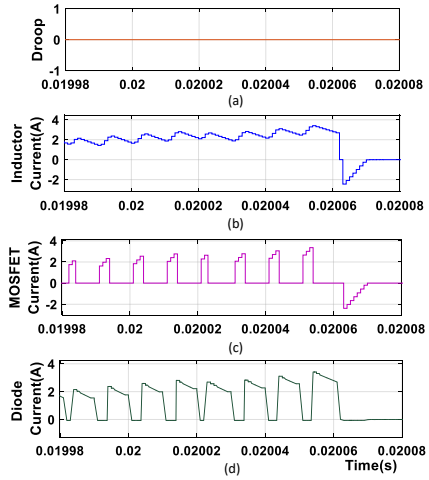

Fig. 12. Converter-1 results for fault F_1 at 0.02 s without proposed algorithm (a) Adaptive droop value (b) Source current (c) MOSFET current (d) Diode current.

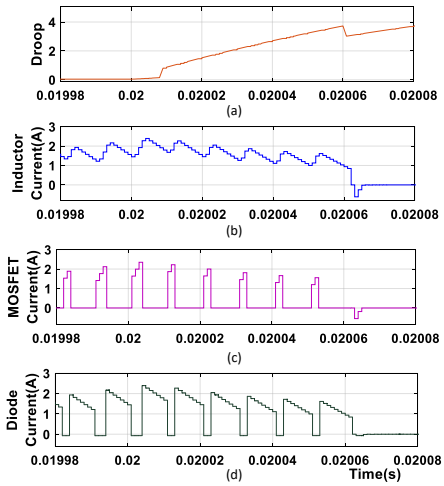

Fig. 13. Converter-1 results for fault F_1 at 0.02 s with proposed algorithm (a) Adaptive droop value (b) Source current (c) MOSFET current (d) Diode current.

algorithm are shown in Fig. 14(a, b). In this case the total time taken to clear the fault is approximately 205 μs as shown in Fig. 14(b). Fig. 15(a, b) shows the fault clearing time with the proposed adaptive droop control. The droop adjusts the source current, and hence it gives an additional time to reach the threshold. In this case the total time taken by the fault current to cross the threshold is approximately 265 μs. From the above results and discussions, it can be concluded that with the proposed algorithm an additional 60 μs is available to clear the fault.

C. Feeder fault (F2)

At 0.025 s a line-line fault (F2) is initiated and the simulation results are shown in Fig. 16. It can be observed from Fig. 16 (b, d) that the DCCB isolates the feeder from the system as soon as the feeder current magnitude is above the upper threshold of 10 A.

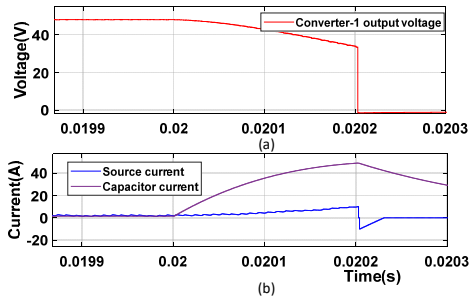

Fig. 14. Converter-1 results for fault F_1 at 0.02 s without proposed algorithm (a) Output voltage (b) Source and capacitor currents.

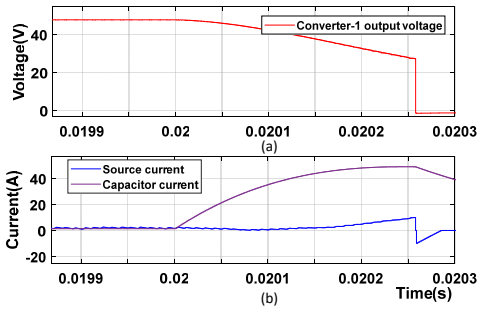

Fig. 15. Converter-1 results for fault F_1 at 0.02 s at 0.02 s with proposed algorithm (a) Output voltage (b) Source and capacitor currents.

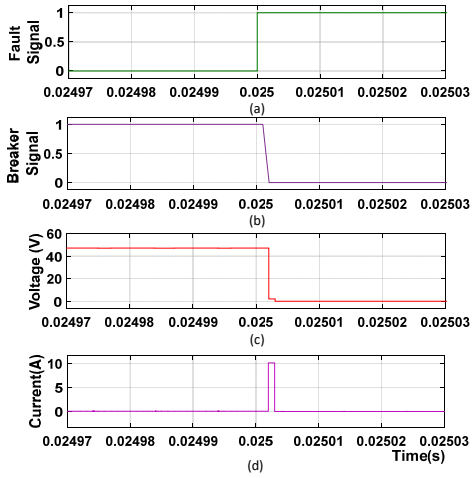

Fig. 16. Results for fault F_2 at 0.025 s (a) Fault signal (b) Breaker signal (c) Feeder voltage (d) Feeder current.

V. Conclusion

Problems like fault clearing time and the bus voltage fluctuation during faults or disturbances will affect the safe operation of the DC microgrids. To address these concerns, in this paper an adaptive droop algorithm for a low voltage DC microgrid is proposed. This method uses voltage and current thresholds to localize the fault. After locating the fault, the proposed method controls the source current instantaneously by adjusting the converter output voltage using virtual resistance R_{droop}. It is also found that the proposed algorithm gives an additional time of 60 μs to clear the fault, and it helps the controller to operate the corresponding DCCB safely. Therefore, the analysis and results indicate that the proposed method is also suitable for the islanded DC microgrids with communication.

Acknowledgment

Sandia National Laboratories is a multimission laboratory managed and operated by National Technology & Engineering Solutions of Sandia, LLC, a wholly owned subsidiary of Honeywell International Inc., for the U.S. Department of Energys National Nuclear Security Administration under contract DE-NA0003525.

References

[1] J. Guerrero, A. Davoudi, F. Aminifar, J. Jatskevich, and H. Kakigano, "Guest Editorial: Special section on smart DC distribution systems," *IEEE Trans. Smart Grid*, vol. 5, no. 5, pp. 2473–2475, Sept. 2014.

[2] S. Augustine, M. K. Mishra, and N. Lakshminarasamma, "Adaptive droop control strategy for load sharing and circulating current minimization in low-voltage standalone DC microgrid," *IEEE Trans. on Sust. Energy*, vol. 6, no. 1, pp. 132–141, Jan 2015.

[3] V. Nasirian, S. Moayedi, A. Davoudi, and F. Lewis, "Distributed cooperative control of DC microgrids," *IEEE Trans. Power Electron.*, vol. 30, no. 4, pp. 2288–2303, Apr. 2015.

[4] D. M. Bui, S. Chen, C. Wu, K. Lien, C. Huang, and K. Jen, "Review on protection coordination strategies and development of an effective protection coordination system for DC microgrid," in *2014 IEEE PES Asia-Pacific Power and Energy Engineering Conference (APPEEC)*, Dec 2014, pp. 1–10.

[5] T. Dragicevic, J. Vasquez, J. Guerrero, and D. Skrlec, "Advanced LVDC electrical power architectures and microgrids: A step toward a new generation of power distribution networks." *IEEE, Electri. Mag.*, vol. 2, no. 1, pp. 54–65, Mar. 2014.

[6] B. Subudhi and R. Pradhan, "A comparative study on maximum power point tracking techniques for photovoltaic power systems," *IEEE Trans. Sust. Energy,*, vol. 4, no. 1, pp. 89–98, Jan. 2013.

[7] R. M. Cuzner and G. Venkataramanan, "The status of DC micro-grid protection," in *2008 IEEE Industry Applications Society Annual Meeting*, Oct 2008, pp. 1–8.

[8] S. Augustine, J. E. Quiroz, M. J. Reno, and S. Brahma, "DC microgrid protection: Review and challenges," in *Sandia National Laboratories, SAND2018-8853, 2018.*

[9] J. Park and J. Candelaria, "Fault detection and isolation in low-voltage DC-bus microgrid system," *IEEE Trans. on Power Delivery*, vol. 28, no. 2, pp. 779–787, April 2013.

[10] S. Dhar, R. K. Patnaik, and P. K. Dash, "Fault detection and location of photovoltaic based DC microgrid using differential protection strategy," *IEEE Trans. on Smart Grid*, vol. 9, no. 5, pp. 4303–4312, Sept 2018.

[11] C. Yuan, M. A. Haj-ahmed, and M. S. Illindala, "Protection strategies for medium-voltage direct-current microgrid at a remote area mine site," *IEEE Trans. on Ind. Appli.*, vol. 51, no. 4, pp. 2846–2853, July 2015.

[12] L. Zhang, N. Tai, W. Huang, J. Liu, and Y. Wang, "A review on protection of DC microgrids," *Journal of Modern Power Systems and Clean Energy*, vol. 6, no. 6, pp. 1113–1127, Nov 2018.

[13] E. Christopher, M. Sumner, D. W. P. Thomas, X. Wang, and F. de Wildt, "Fault location in a zonal DC marine power system using active impedance estimation," *IEEE Trans. on Ind. Appli.*, vol. 49, no. 2, pp. 860–865, March 2013.

[14] D. Thomas, M. Sumner, D. Coggins, X. Wang, J. Wang, and R. Geertsma, "Fault location for DC marine power systems," in *2009 IEEE Electric Ship Technologies Symposium*, April 2009, pp. 456–460.

[15] R. Mohanty, U. S. M. Balaji, and A. K. Pradhan, "An accurate non-iterative fault-location technique for low-voltage DC microgrid," *IEEE Trans. on Power Deli.*, vol. 31, no. 2, pp. 475–481, April 2016.

[16] J. Wang, B. Berggren, K. Linden, J. Pan, and R. Nuqui, "Multi-terminal DC system line protection requirement and high speed protection solutions," *CIGRE International Symposium*, pp. 1–9, 2015.

[17] S. Augustine, N. Lakshminarasamma, and M. K. Mishra, "Control of photovoltaic-based low-voltage DC microgrid system for power sharing with modified droop algorithm," *IET Power Elect.*, vol. 9, pp. 1132–1143(11), May 2016.